Study on Collision Between Two Ships Using Selected Parameters in Collision Simulation

Dong-Myung Bae[1], Aditya Rio Prabowo[1,2,3] *, Bo Cao[1], Ahmad Fauzan Zakki[4] and Gunawan Dwi Haryadi[3]

1. Department of Naval Architecture and Marine Systems Engineering, Pukyong National University, Nam-gu Daeyon Busan 48513, Republic of Korea
2. Interdisciplinary Program of Marine Convergence Design, Pukyong National University, Nam-gu Daeyon Busan 48513, Republic of Korea
3. Department of Mechanical Engineering, Diponegoro University, Semarang, Central Java 50275, Republic of Indonesia
4. Department of Naval Architecture, Diponegoro University, Semarang, Central Java 50275, Republic of Indonesia

Abstract: In the present analysis, several parameters used in a numerical simulation are investigated in an integrated study to obtain their influence on the process and results of this simulation. The parameters studied are element formulation, friction coefficient, and material model. Numerical simulations using the non-linear finite element method are conducted to produce virtual experimental data for several collision scenarios. Pattern and size damages caused by collision in a real accident case are assumed as real experimental data, and these are used to validate the method. The element model study performed indicates that the Belytschko-Tsay element formulation should be recommended for use in virtual experiments. It is recommended that the real value of the friction coefficient for materials involved is applied in simulations. For the study of the material model, the application of materials with high yield strength is recommended for use in the side hull structure.

Keywords: ship collision, collision accident, non-linear finite element, collision parameter, hull structure

1 Introduction

Ship transport is essential for transporting people and products between islands in the Indonesian archipelago. One of the busiest shipping routes is the Merak (Province of Banten) to Bakauheni (Province of Bengkulu) route through the Sunda Strait, where, in a section of the strait, traffic traveling from east to west (from Java to Sumatra) crosses traffic traversing from north to south (Batam, Singapore, to the Indian Ocean). Thus, accidents frequently occur in this area; two accidents have occurred in the past three years between 2012 and 2014, and the most recent of which was a collision between a roll-on-roll-off (ro-ro) passenger ship and general cargo ship in May 2014. In the marine and naval community, there is an increasing demand for the reduction in ocean pollution and vessel losses that occur in relation to such accidents. The tragic losses of numerous ro-ro passenger ships such as the European Gateway in 1982, the Herald of Free Enterprise in 1987, and particularly, the catastrophe of the Estonia in 1994 with the loss of more than 800 lives have led many countries to reassess passenger ship safety. In addition, collision and grounding significantly contribute to ship structural damage, and according to the statistics of Lloyd's Register on 1995, collision and grounding of ships are responsible for nearly half of all ship losses (Zhang, 1999a).

In recent years, there have been improvements and developments in simulations and analyses of ship collisions. Such work began with the use of the empirical formula of Minorsky for determining the energy absorbed by a ship structure during collision (Minorsky, 1959). This was followed by Zhang (1999b), who provided an illustration of coordinates involved in the external dynamics of ship collisions, and then Kitamura (2002), who applied the Finite Element (FE) approach in a collision and grounding simulation. The results of previous research indicate that the use of the FE approach for conducting collision simulation and analysis in a virtual experiment is adequate for calculating and producing results that agree with simplified analysis or real experiment results. However, several parameters are involved when the FE method is applied in virtual experiments, and these parameters affect the results.

This paper presents an integrated study of parameters involved in collision simulations with the aim of predicting the influence of such parameters on the results of a numerical simulation of ship collisions. The parameters investigated in the integrated study are limited to element formulation, friction coefficient, and material model.

2 Collision research review

FE analysis has previously been used in full-scale experiments and collision accident studies, and numerous

studies on ship collisions have been performed by scientists and other authorities. For example, a comparative study was performed on the structural integrity of single and double side skin bulk carriers under collision damage, in addition to the numerical modeling of ship collision based on FE codes by Ozguc *et al.* (2005). Moreover, the FE method has been applied in the simulation of collision and grounding damages (Kitamura, 2005). Furthermore, a ship collision study by Pedersen and Zhang (2000) determined the effect of ship structure and size on grounding and collision damage distributions, and Wiśniewski and Kolakowski (2003) mentioned the effects of selected parameters such as ship velocity on ship collisions. The bending stress of a ship's hull during ship collision was determined by Pedersen and Li (2009), and numerous ship collision simulations based on collision types have been studied by Haris and Amdhal (2013). Research related to energy absorption by a ship structure during collision was performed by Lehmann and Pechmann (2002), and in this respect, a study of the internal mechanic modeling during ship collision was conducted by Paik and Pedersen (1996). Based on the work of Kitamura (2002), improvements have now been made in the accuracy and practicality of the FE method, particularly when data from real accidents, physical experiments, and/or the use FE analysis, i.e., numerical experiments, are employed.

3 Theory and methodology review

The most practical method currently employed for conducting analyses and simulations of collisions is the FE method using numerical simulations, which are divided into linear and non-linear simulations. Non-linear analysis is applied as a method to calculate stresses and deformations of products under the most general loading and material conditions, for example, with dynamic (time-dependent) loads; large component deformations; and non-linear materials such as rubber or metals, beyond their yield point. Non-linear analysis is a more complex approach but results in a more accurate solution than linear analysis when the basic assumptions of linear analysis are violated. The application of an algorithm in both linear and non-linear analysis can also be significant depending on the type of simulation. In the present study, Lagrange multiplier algorithm or augmented Lagrange is used in collision simulation. In the classical Lagrange multiplier method, contact forces are expressed by Lagrange multipliers, whereas the augmented Lagrange method involves the regularization of the classical Lagrange method by adding a penalty function from the penalty method (Simo and Laursen, 1992). This method, unlike the classical one, can be used for sticking friction, sliding friction, and frictionless contact conditions. An illustration of the concept of this algorithm is presented in Fig. 1. The representation of the contact problem, which involves the minimization of potential Π, is presented in Eqs. (1)–(3) as follows:

Fig. 1 Contact element in Lagrangian method

$$\Pi(u,\Lambda) = \Pi_A(u) + \Lambda^T g + \frac{1}{2} g^T k g \qquad (1)$$

$$\Lambda^T = \left[\left\{ \begin{matrix} \lambda_n^1 \\ \lambda_t^1 \end{matrix} \right\}, \left\{ \begin{matrix} \lambda_n^2 \\ \lambda_t^2 \end{matrix} \right\}, \ldots \left\{ \begin{matrix} \lambda_n^k \\ \lambda_t^k \end{matrix} \right\}\right] \qquad (2)$$

$$g = \left[\left\{ \begin{matrix} g_n^1 \\ g_t^1 \end{matrix} \right\}, \left\{ \begin{matrix} g_n^2 \\ g_t^2 \end{matrix} \right\}, \ldots \left\{ \begin{matrix} g_n^k \\ g_t^k \end{matrix} \right\}\right] \qquad (3)$$

where λ_n is the Lagrange multiplier for the normal direction, λ_t is the Lagrange multiplier for the tangential direction, g_n is penetration along the normal direction, and g_t is penetration along the tangential direction.

The augmented Lagrange is basically the same as the penalty method, but the λ_i constant is added to the augmented Lagrange, which makes this algorithm extremely accurate [13]. The equations for these algorithms are as follows:

$$\delta\Psi = \int_V \sigma^T \delta\varepsilon dV + \int_\Gamma (\varepsilon_N g_N \delta g_N + \varepsilon_T g_T \delta g_T) dA \qquad (4)$$

$$\Delta F_{cont.} = K_{cont.} \Delta x_{penetr} \qquad (5)$$

$$\delta\Psi = \int_\Gamma [(\lambda_N + \varepsilon_N g_N)\delta g_N + (\lambda_T + \varepsilon_T g_T)\delta g_T] dA \qquad (6)$$

$$\lambda_{i+1} = \lambda_i + K_{cont.} \Delta x_{penetr.} \qquad (7)$$

where $F_{cont.}$ is the contact force, $K_{cont.}$ is the contact stiffness, $x_{penetr.}$ is the distance between two existing nodes on separate contact bodies, and λ_i is the Lagrange Multiplier.

Collision analysis has undergone many developments and improvements since its introduction and can be classified into four categories: empirical, simplified, experiment, and FE methods. Empirical methods were introduced and developed in past research. In the present study, Zhang's empirical formula method is considered. Proposed formula is using empirical formula from Zhang which the formula implementation is divided into crushing and folding as well as tearing damage mode. These formula for two deformation modes i.e. crushing and folding as well as tearing are presented on Eqs. (8) and (9) consecutively (Zhang, 1999c).

$$E = 3.50 \left(t/d\right)^{0.67} \sigma_0 R_T \qquad (8)$$

$$E = 3.21 \left(t/l\right)^{0.6} \sigma_0 R_T \qquad (9)$$

where E is the absorbed energy (MJ), σ_0 is the height of the rupture aperture in the side shell (m), t is the average thickness of the crushed plate (mm), d is the average width of plates in the crushed cross-section (mm), l is the critical tearing length (mm), and R_T is the destroyed volume of material (m³).

4 Real accident study

The study is divided into two main parts: the study of a real collision accident, which is discussed in this section, and the study of parameters influencing the collision process, which is discussed in a later section. The study of a real accident is conducted to verify the method used in our virtual experiment. As a real ship collision experiment is very expensive to conduct, a previous real ship collision accident is considered as a real experiment, and this is modeled and analyzed using the non-linear FE method to obtain virtual experiment results. The damage characteristics from the real collision accident are considered as real experimental results, and these are used to validate the numerical simulation. In addition to real damage, empirical formulae are used to verify the method. The method verified in the first part of the study is then used for the integrated study in the second part.

4.1 Collision scenario of a real accident

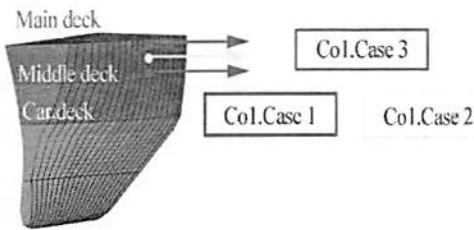The accident occurred on 3 May, 2014 at around 02:25 local time, between the islands of Sumatra and Java in the Sunda Strait. An Indonesian ro-ro passenger was severely damaged after being stuck by a reefer ship, where the reefer struck the starboard side of the ro-ro ship at a velocity of 12 knots between the main and middle decks, and caused a rip with a length and width of approximately 7 m and 5 m, respectively, with a penetration depth of approximately 2.5 m.

4.2 Collision case scenario for numerical simulation

Three collision cases are performed in the present study, and each is determined and selected based on possible contact points involved in the actual accident. Details of contact points are all longitudinal at frame number 106, and then vertical at 9.31 m, 10.25 m, and 11.19 m from the baseline; they are named Collision Cases 1, 2, and 3 respectively. During the collision process, the ramming ship struck the proposed target points at a velocity of 12 kn (6.17 m/s), while the struck ship is set to be fixed at the centerline with the end of the model are clamped as the boundary condition. An illustration of the contact points and collision process are presented in Fig. 2 and 3, respectively.
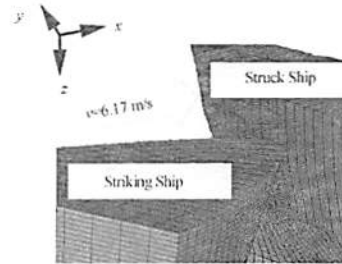

Fig. 2 Illustration of contact point for proposed collision case

Fig. 3 Illustration of collision process

4.3 Definition of ships involved

This collision accident involved two ships; the ro-ro passenger ship was struck by the reefer ship. The configurations and main dimensions of these ships are presented in Tables 1 and 2.

In the virtual experiment process, the struck ship is considered as a deformable structure and the striking ship as a rigid body. Only one half-hull of the struck ship is modeled to reduce CPU time. The models of the struck and striking ships are presented in Fig. 4.

Table 2 Main dimensions of striking ship

Characteristic	Type and value
Type of ship	Reefer
Length overall / m	144.50
Breadth moulded / m	19.80
Design draft / m	5.60
Depth / m	10.20

Table 1 Configuration of struck ship

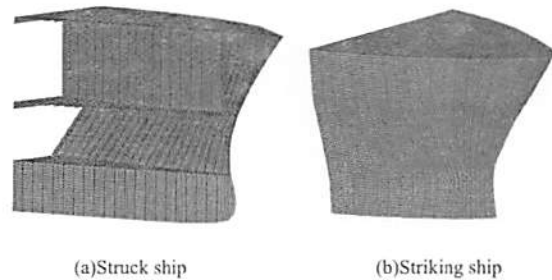| Characteristic	Type and value
Type of ship	Ro-ro passenger
Length overall / m	85.92
Length between perpendicular / m	78.00
Breadth moulded / m	15.00
Design draft / m	4.30
Depth / m	10.40
Frame spacing / m	0.60
Space between outer and inner shell / m	3.50

(a)Struck ship   (b)Striking ship

Fig. 4 Ships involved in collision

The element choice in the present research is that of the Belytschko-Tsay element. Alsos and Amdahl (2007) and Tornqvist and Simonsen (2004) both suggested that the element-length-to-thickness (ELT) ratio should be within a range of 5–10, so that the local stress and strain fields can adequately captured. A fine mesh with a size of 80 mm is applied to the core area of the struck ship, and fine meshes measuring 90 mm and 100 mm are applied to the transitional and outside areas, respectively. The element-length-to-thickness (ELT) ratio for this area is in the range of 8–10. The area for the striking ship model is divided into two parts: the first area experiences direct contact with the struck ship, and a fine mesh with a size of 340 mm is applied; the second is the remaining area, where a fine mesh with a size of 680 mm is applied. The simulation considers the struck ship as a deformable structure and the striking ship as a rigid body, and the virtual experiment model consists of about 74 023 elements; the total computation time for all virtual experiments varies between 9 and 72 h on a computer with the following specifications: 4th Generation Intel Core i7-4790 Processor 4.00 GHz with 16 GB RAM.

4.4 Material definition

To obtain the most similar material properties to those of the real ships' materials, hardness and chemical composition test are conducted. These tests are performed using a material sample from the side shell of the struck ship (ro-ro passenger ship). Hardness tests are performed using the ASTM E18-05[r-1] test method with a test type Rockwell Hardness Number (HRA) load test of 0.588 kN (ASTM International, 2006). The test for chemical composition was conducted using a WAS/PMI-MASTER Pro spectrometer from Oxford Instruments (Oxford Instruments Analytical, 2013).

Results and comparisons of predicted materials from both tests are presented in Tables 3 and 4. After comparing the results of tests with those from theory and other material characteristics obtained in a literature review (Callister Jr., 2007), it can be concluded that the sample of the struck ship material is composed of plain medium carbon steel, type AISI 1030. However, there are differences in the sulfur composition in relation to a previous repair of the ship's hull, but other compositions give a good correlation between the ship's material and AISI 1030. A list of the model's material used as a reference in the numerical simulation is presented in Table 5. A plastic-kinematics material is considered in the analysis, and the yield function of the plastic-kinematics material is given as Eqs. (10) and (11),

$$\sigma_y = \left[1 + \left(\frac{\varepsilon}{C}\right)^{\frac{1}{P}} \right] \left(\sigma_0 + \beta \, E_p \varepsilon_p^{eff} \right) \qquad (10)$$

$$E_p = \frac{E_{tan} E}{E - E_{tan}} \qquad (11)$$

where σ_y is the yield stress (Pa), ε is the strain rate (s^{-1}), C is the Cowper-Symonds strain rate parameter (s^{-1}), P is the

Cowper-Symonds strain rate parameter, σ_0 is the initial yield stress (Pa), β is the hardening parameter, E_p is the plastic hardening modulus (Pa), E_{tan} is the tangent modulus (Pa), E is Young's modulus (Pa), and E_p^{eff} is the effective plastic strain.

Table 3 Results of hardness test

Test Mode	Symbol	Hardness	
		Ship Material	AISI 1030
Hardness Rockwell A	[HRA]	50.37	
Hardness Rockwell B	[HRB]	81.49	80
Hardness Vickers	[HV]	154.35	155

Table 4 Results of chemical composition test / %

Element	Symbol	Composition	
		Ship Material	AISI 1030
Iron	[Fe]	98.6000	98.67–99.13
Manganese	[Mn]	0.8480	0.60–0.90
Carbon	[C]	0.2900	0.27–0.34
Phosphorous	[P]	0.0340	≤0.04
Sulfur	[S]	0.0954	≤0.05

Table 5 Material model

Properties	Symbol	Value
Density /(kg·m^{-3})	[ρ]	7850
Young's modulus / MPa	[EX]	210000
Poisson's ratio	[NUXY]	0.30
Yield stress / MPa	[σ_yt]	440
Hardening parameter		0
Strain rate /(s^{-1})	[C]	3200
Strain rate	[P]	5
Failure strain		0.20

4.5 Finite element procedure

The real phenomena involved in the ship collision accident are considered to be the real experiment, and these are modeled and analyzed using a numerical simulation to obtain virtual experiment results. The results of the virtual experiment are then compared with those of the real experiment, and the empirical formula calculations used to verify the method in the virtual experiment are validated. Numerical simulations use the non-linear FE method as a solution method, and the augmented Lagrange is chosen as the contact algorithm used in numerical simulations. Details of the procedures and processes used in this paper are presented in Fig. 5.
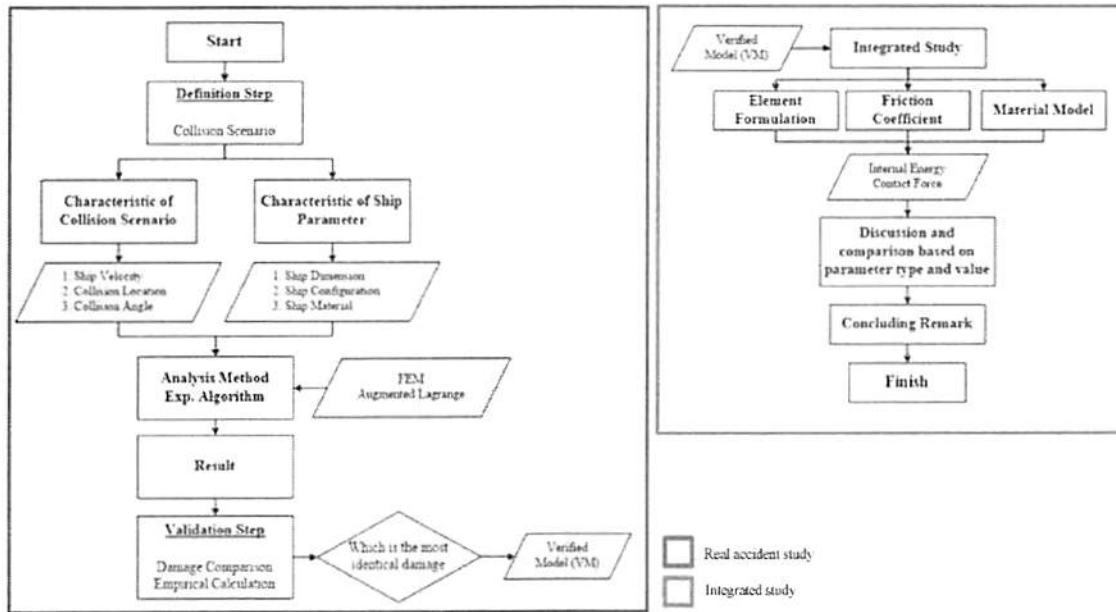
Fig. 5 Diagram of the procedure used in this study

4.6 Results and discussion of accident investigation

Results of virtual experiments using the non-linear FE method are presented in this section; the damage pattern of the three cases are presented in Figs. 6 to 8. Fig. 6, which shows Collision Case 1, indicates that neither the edge part of the main deck nor most of the side shell were destroyed during the collision process; the side shell was only torn near the middle deck. The damage in Collision Case 2 indicates that the side shell was torn and destroyed during the collision process, and that the edge part of the main deck was deformed. Collision Case 3 shows that both the side shell and the main deck were destroyed during the collision process. The list of damage determined in virtual experiments, and a comparison with those of the real accident, are presented in Figs. 9 and 10, and in Table 6.
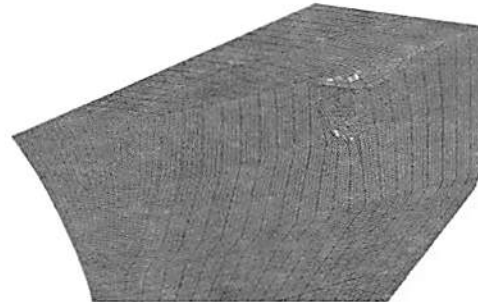
Fig. 7 Damage pattern in Collision Case 2
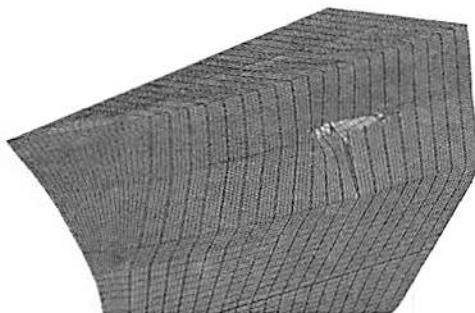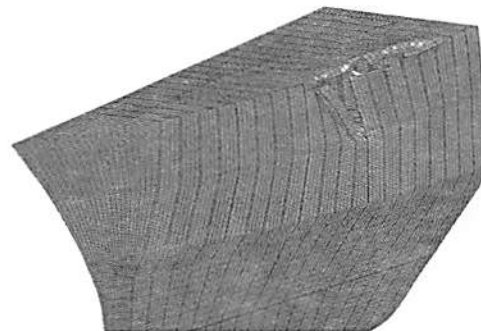

Fig. 6 Damage pattern in Collision Case 1

Fig. 8 Damage pattern in Collision Case 3

(a) Case 2-diagonal view
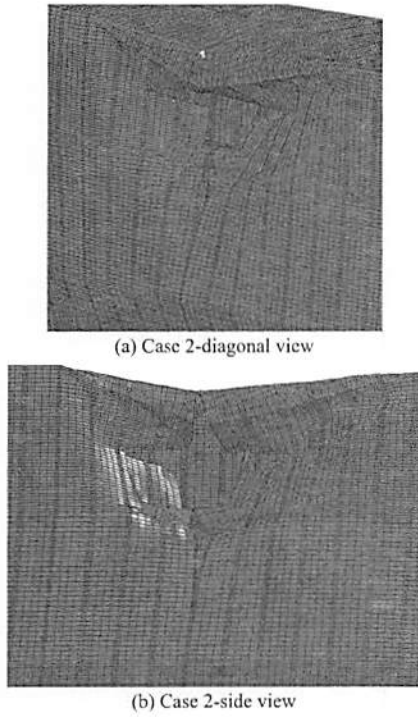

(b) Case 2-side view

Fig. 9 Damage pattern

Fig. 10 Damage pattern of real collision accident

A comparison of the damage pattern shown in Figs. 6 to 10, and the summary given in Table 6, concludes that the virtual experiment for Collision Case 2 produces the most similar damage to that of the real accident. Therefore, the configuration and location of the collision spot in Collision Case 2 are used and applied in an integrated study to investigate the influence of several selected parameters on the internal energy and contact force that occurred during the collision process, and which are used in this study (as presented in Figs. 11 and 12, respectively).

Table 6 Summary and comparison of damage

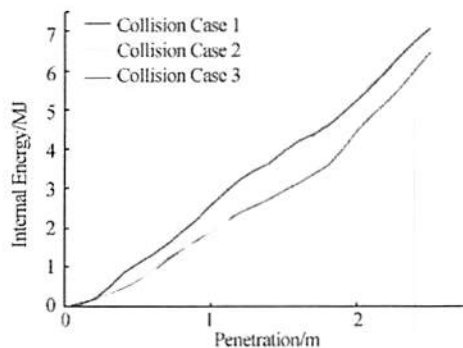| Case No.	Deformation size		Deformation type			
	Length/m	Width/m	Side shell	Frame	Middle deck	Main deck
1	4.20	5.00	Torn	Torn	Deformed	Deformed (Side part)
2	7.00	4.50	Destroyed	Destroyed	Deformed	Deformed (Side part)
3	7.00	3.00	Destroyed	Destroyed	Deformed	Destroyed (Side part)
Actual	7.00	5.00	Destroyed	Destroyed	Deformed	Deformed (Side part)

Fig. 11 Internal energy vs. penetration graph

Differences in internal energy between all the cases are in the range of 2%–9%; internal energy in Collision Case 1 is 2.18% bigger than that in Collision Case 2, and 8.54% bigger than in Collision Case 3 at the end of the collision process. Fig. 11 also indicates that the structure involved in Collision Case 1 has the best ability to absorb collision energy during the collision process compared with the structure in the other collision cases.
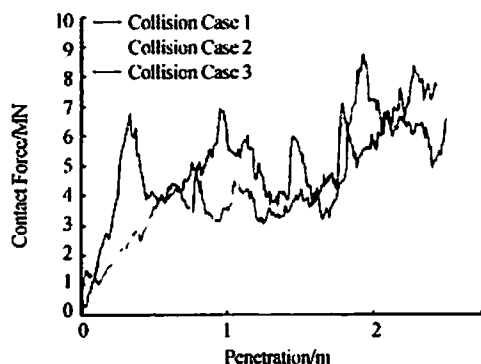
Fig. 12 Contact force vs. penetration graph

The contact force vs. penetration graph indicates the amount of force needed to deform or even destroy the structure during the collision process. The average force indicates that the structure in Collision Cases 2 and 3 needs less force to destroy it during the collision process than that in Collision Case 1. The results from the virtual experiment are verified using the empirical formula from Zhang, which is recommended for use because the formulae are divided into several formulas dependent on deformation type. These formulae are considered practical in application, and have good correlations with the virtual experiments. Results of the calculation of empirical formulae and their comparison with the virtual experiment results are presented in Table 7.

Table 7 Results of experiment and empirical formula

Case no.	Contact force / MN	Internal energy / MJ	
		Virtual exp.	Zhang
1	4.89	7.07	7.43
2	4.64	6.91	6.97
3	4.43	6.46	6.48

5. Integrated study

A series of virtual experiments using the method verified from previous study are conducted using several selected parameters involved in the both the real accident and the numerical simulation. The influence of these parameters on the results of virtual experiments are then presented and discussed.

5.1 Element formulation

There are many types of element formulations that can be applied to models in numerical simulations. Each type of element contributes to the results of calculations and analysis. Four element types are selected for application to the model and are investigated in this section: the Hughes-Liu (HL), Belytschko-Levithan (BL), Belytschko-Wong Chiang (BWC) and the Belytschko-Tsay (BT). Results of virtual experiments can be seen in Figs. 13 and 14 for internal energy and contact force, respectively. It can be seen from Fig. 10, that there is no significant difference in

terms of the internal energy for all proposed element formulations, which is below 5%, as is that of contact force.
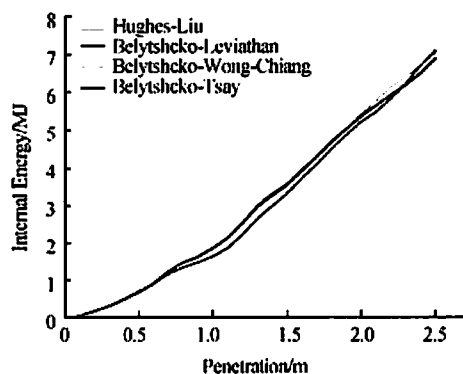

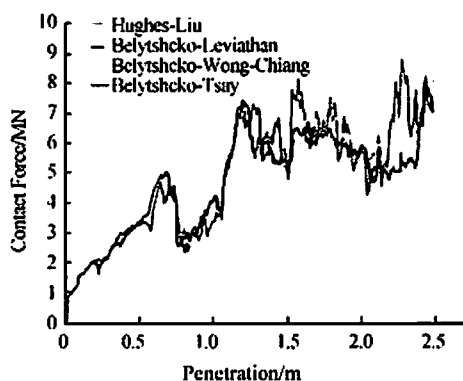Fig. 13 Influence of element formulations on internal energy

Fig. 14 Influence of element formulations on contact force

Although there is no significant difference in terms of internal energy and contact force, there is a significant difference in terms of the virtual experiment time taken. The BT method produced the fastest results among all the proposed element formulation, followed by the BL method, which was 25% slower. Element formulation for the HL method produced the slowest results of all other element formulation types, with a difference of approximately 50%. Therefore, the BT method was the fastest, although there was no significant difference between use of the HL and the BWC methods (7.38x10^{-3}%). Details of the time simulations from four element formulation types are presented in Fig. 15, where the HL element formulation is based on a degenerated continuum formulation, which results in substantially large computational costs but is effective when very large deformations are expected. However, although the entire results of the study on element formulation determined no significant result, the application of BT element formulation is recommended to reduce time involved in the virtual experiment; it also produces confident results.

5.2 Friction coefficient

Past authors have not always revealed their application of the friction coefficient for friction between materials in ship

collision analysis (Kitamura, 2002; Haris and Amdahl, 2013; Alsos and Amdahl, 2007). In engineering practice, both the static and dynamic friction coefficients, equal to 0.3, are used in most cases, and values of coefficient larger than 0.6 are rarely used. In this study, the collision case study from the previous section is used as a study object, and influences of the different values of the friction coefficient are taken as the main focus. Values of the friction coefficient equal to 0.4, 0.5, 0.6, and 0.7 are thus investigated and compared with the result, using engineering practice with a value of 0.3 and friction between mild steels with values of 0.74 and 0.57 for static and dynamic friction, respectively. Identical values of the other parameters were used to obtain the specific effect from this parameter. Fig. 16 shows how the value of the friction coefficient effects the results of absorbed energy of the structure during the collision process. This figure indicates that there are no significant differences for friction coefficient values 0.4 and 0.5, or for engineering practices with a value of 0.3. However, a significant difference of approximately 8% is seen between friction coefficients 0.5 and 0.6, although no significant difference is seen after 0.6.

Results on internal energy also indicate that application of the real friction coefficient of the material involved in the contact process produces better results than the friction coefficient value of engineering practice, which produces a smaller amount of internal energy. In terms of the contact force in Fig. 17, significant differences in the average force are also spotted between values 0.5 and 0.6, with a difference of approximately 9%. It can therefore be concluded, that the effect of friction coefficients have a smaller effect between values of 0.3–0.5 and 0.6–0.74. However, a significant effect is apparent when the friction coefficient value is replaced by 0.6.

5.3 Material model

The material model is an absolute parameter that is involved in every type of simulation. The results of a study based on real phenomena can be developed and improved if the specific material model, based on a real experiment test or phenomena, is used in the virtual experiment. Four materials, based on real materials generally used on a ship, are proposed as references for the material model, and these are investigated in this section; the mechanical properties for each material are presented in Table 8. These material references are chosen based on their class and yield strength. AISI 1018 is taken as a sample for a class of plain low carbon steel, AISI 1030 for a plain medium carbon steel, and AH32 and AH36 for low alloy high strength materials.
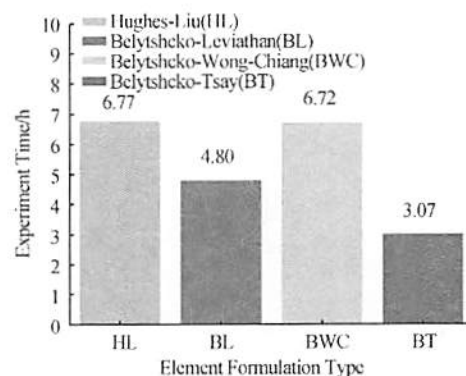

Fig. 15 Experiment time involved in element formulations

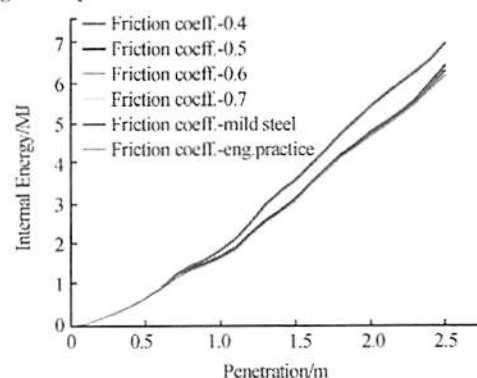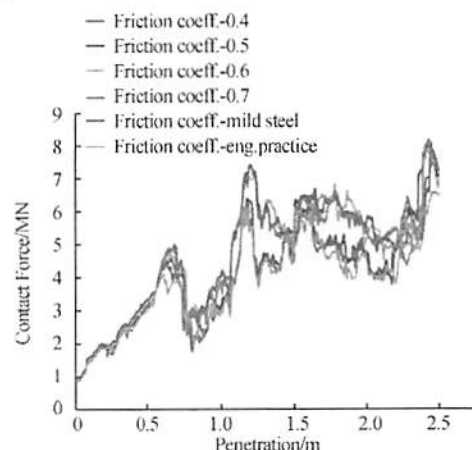Fig. 16 Influence of friction coefficient on internal energy

Fig. 17 Influence of friction coefficient on contact force

Table 8 Material properties

Properties	Symbol	Value			
		1018	1030	AH32	AH36
Density / (kg·m^{-3})	$[\rho]$	7 865	7 850	7 850	7 850
Young's modulus / MPa	$[EX]$	200 000	210 000	200 000	200 000
Poisson's ratio	$[NUXY]$	0.27	0.30	0.29	0.29
Yield strength / MPa	$[\sigma_{ys}]$	310	440	315	350
Ultimate tensile s. / MPa	$[\sigma_{uts}]$	440	525	585	620

The effect of material models on the internal energy-penetration and contact force-penetration curves are presented in Figs. 18 and 19, respectively. It can be concluded from T, that the material type AISI 1030 from the medium-carbon steel class has the best ability, in terms of absorbed energy, during the collision process. In contrast, material type AH32 from the low-alloy class absorbed the smallest amount of energy out of all proposed materials. The differences for both internal energy and contact force between all the materials range between 16% and 26%. Comparing the results of the virtual experiment and the mechanical properties of the material, the amount of energy absorbed by the material during the collision process is directly proportional to the yield strength of the material itself.
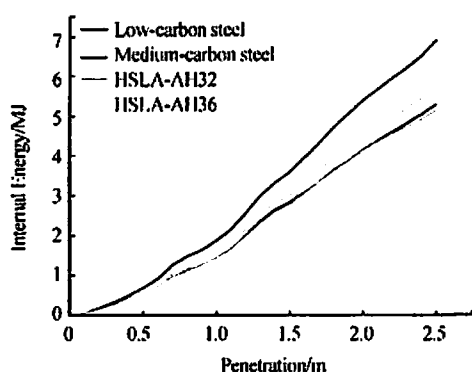

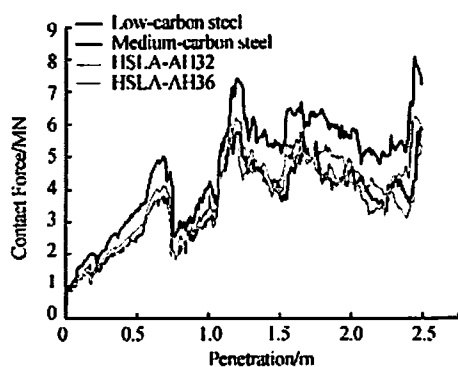**Fig. 18 Influence of material model on internal energy**

Fig. 19 Influence of material model on contact force

The use of material type AH32 as the material model, which has a yield strength value of 315 MPa, absorbs less energy than AISI 1030, which has a yield strength of 440 MPa. The result of the average contact force also indicates that a high force is required to deform or destroy the structure of AISI 1030, which has the highest yield strength. The exception occurs when the difference in yield strength between materials as presented in Table 8 is below 2%. Other material properties, such as Poisson's ratio and density, will also affect the result of the experiment. This exception can be seen in material types AH32 and AISI 1018. It is clear that

AH32 has a higher yield strength than AISI 1018, but the result of average internal energy and contact force indicates that AISI 1018 has a better ability to absorb energy, and that it requires a greater force to deform or destroy it.

6 Concluding remarks

This paper presents a study and associated results relating to a number of parameters used in virtual simulations of collisions. Investigation and analysis in relation to the prediction and effect of these parameters on the virtual experiment are the main focus of this paper. A real collision accident is studied, and an empirical method is used to validate the study and configuration of the numerical simulation.

Element formulation delivers good results when used in time simulations. The Belytschko-Tsay element formulation is recommended for use in virtual experiments, as it reduces computational time; however, the Hughes-Liu method is preferred for large deformations.

Influence of the friction coefficient is very significant at values between 0.5 and 0.6, whereas the effects below 0.5 and above 0.6 are less significant. A comparison between the value of engineering practice and the real coefficient value of friction between mild steel is presented, and the difference is found to be below 20% for both absorbed energy and contact force. If no instructions are provided when performing a virtual experiment using a specific friction coefficient, the real value of the friction coefficient between contact materials is recommended for use in the simulation instead of friction coefficient for engineering practice.

In the study of the material model, the application of materials with a high yield strength is recommended for use in the side of a hull's structure. The exception occurs when there is a difference in the yield strength of below 2%. There is a demand for developing and improving application of material types in a ship structure, particularly for the side of the hull. The writer therefore recommends further study of the influence of specific mechanical properties in collisions.

References

Alsos HS, Amdahl J, 2007. On the resistance of tanker bottom structures during stranding. *Journal of Marine Structure*, 20, 218-237.
DOI: 10.1016/j.marstruc.2007.06.001

ASTM International, 2006. *ASTM E18-15 standard test methods for rockwell hardness of metallic materials*. ASTM International, West Conshohocken, USA.

Callister Jr. WD, 2007. *Material science and engineering: an introduction, Seventh ed*. John Wiley & Sons, Hoboken, USA, 359-364.

Haris S, Amdhal J, 2013. Analysis of ship-ship collision damage accounting for bow and side deformation interaction. *Journal of Marine Structures*, 32, 18-48.
DOI: 10.1016/j.marstruc.2013.02.002

Kitamura O, 2002. FEM approach to the simulation of collision and grounding damage. *Journal of Marine Structure*, 15, 403-428.
DOI: 10.1016/S0951-8339(02)00010-2

Lehmann E, Peschmann J, 2002. Energy absorption by the steel structure of ships in the event of collisions. *Journal of Marine Structures*, 15, 429-441.
DOI: 10.1016/S0951-8339(02)00011-4

Minorsky VU, 1959. An analysis of ship collision with reference to protection of nuclear power ships. *Journal of Ship Research*, 3(2), 1-4.

Oxford Instruments Analytical, 2013. *PMI-MASTER pro precise, mobile metal analysis*. Oxford Instruments, High Wycombe, United Kingdom.

Ozguc O, Das PK, Barltrop N, 2005. A comparative study on the structural integrity of single and double skin bulk carriers under collision damage. *Journal of Marine Structures*, 18, 511-547.
DOI: 10.1016/j.marstruc.2006.01.004

Ozguc O, Das PK, Barltrop N, Shahid M, 2006. Numerical

modeling of ship collision based on finite element codes. *International ASRANet Colloquium*, Glasgow, United Kingdom.

Paik JK, Pedersen PT, 1996. Modelling of the internal mechanics in ship collision. *Journal of Ocean Engineering*, 23(2), 107-142.

Pedersen PT, Li Y, 2009. On the global ship hull bending energy in ship collisions. *Journal of Marine Structures*, 22, 2-11.
DOI: 10.1016/j.marstruc.2008.06.005

Pedersen PT, Zhang S, 2000. Effect of ship structure and size on grounding and collision damage distributions. *Journal of Ocean Engineering*, 27, 1161-1179.
DOI: 10.1016/S0029-8018(99)00043-8

Simo JC, Laursen TA, 1992. An augmented lagrangian treatment of contact problems involving friction. *Journal of Comp. Structure*, 42, 97-116.

Ştefancu AI, Melenciuc SC, Budescu M, 2011. Penalty based algorithms for frictional contact problems. *Universitatea Tehnică Gheorghe Asachi din Iaşi*, 3, 54-58.

Tornqvist R, Simonsen BC, 2004. Safety and structural crashworthiness of ship structures; modeling tools and application in design, *International Conference on Collision and Grounding of Ships*, Izu, Japan.

Wiśniewski K, Kolakowski P, 2003. The effect of selected parameters on ship collision results by dynamic FE simulations. *Journal of Finite Elements in Analysis and Design*, 39, 985-1006.
DOI: 10.1016/S0168-874X(02)00143-9

Zhang S, 1999a. *The mechanics of ship collisions*. PhD thesis, Technical University of Denmark, Lyngby, 1-2.

Zhang S, 1999b. *The mechanics of ship collisions*. PhD thesis, Technical University of Denmark, Lyngby, 8.

Zhang S, 1999c. *The mechanics of ship collisions*. PhD thesis, Technical University of Denmark, Lyngby, 196-197.